Structural Engineering and Mechanics, *Vol. 71, No. 4 (2019) 391-405*
DOI: https://doi.org/10.12989/sem.2019.71.4.391

Continuous force excited bridge dynamic test and structural flexibility identification theory

Liming Zhou[1,2] and Jian Zhang*[1,2]

[1]*Jiangsu Key Laboratory of Engineering Mechanics, Southeast University, Nanjing 210096, China*
[2]*School of Civil Engineering, Southeast University, Nanjing 210096, China*

(Received December 10, 2018, Revised March 25, 2019, Accepted April 9, 2019)

Abstract. Compared to the ambient vibration test mainly identifying the structural modal parameters, such as frequency, damping and mode shapes, the impact testing, which benefits from measuring both impacting forces and structural responses, has the merit to identify not only the structural modal parameters but also more detailed structural parameters, in particular flexibility. However, in traditional impact tests, an impacting hammer or artificial excitation device is employed, which restricts the efficiency of tests on various bridge structures. To resolve this problem, we propose a new method whereby a moving vehicle is taken as a continuous exciter and develop a corresponding flexibility identification theory, in which the continuous wheel forces induced by the moving vehicle is considered as structural input and the acceleration response of the bridge as the output, thus a structural flexibility matrix can be identified and then structural deflections of the bridge under arbitrary static loads can be predicted. The proposed method is more convenient, time-saving and cost-effective compared with traditional impact tests. However, because the proposed test produces a spatially continuous force while classical impact forces are spatially discrete, a new flexibility identification theory is required, and a novel structural identification method involving with equivalent load distribution, the enhanced Frequency Response Function (eFRFs) construction and modal scaling factor identification is proposed to make use of the continuous excitation force to identify the basic modal parameters as well as the structural flexibility. Laboratory and numerical examples are given, which validate the effectiveness of the proposed method. Furthermore, parametric analysis including road roughness, vehicle speed, vehicle weight, vehicle's stiffness and damping are conducted and the results obtained demonstrate that the developed method has strong robustness except that the relative error increases with the increase of measurement noise.

Keywords: dynamic test; vehicle-bridge-interaction; continuous excitation; modal scaling factor; flexibility identification

1. Introduction

Structural Health Monitoring (SHM) has been developed over a long time and SHM systems have been installed on many bridges (Lynch 2004; Lynch 2007; Deng and Cai. 2007; Brownjohn *et al*. 2010; Soyoz and Feng 2010; Catbas *et al*. 2013; Adewuyi and Wu 2015; Liu *et al*. 2017; Sabato *et al*. 2017). The vibration-based SHM technology has progressively become a commonly used approach for structure safety evaluation. For instance, the ambient vibration test has been extensively applied for modal identification of several kinds of bridges (Bayraktar *et al*. 2009; Zhang *et al*. 2013; Fujino *et al*.2015; Rahbari *et al*. 2015; Sevim *et al*. 2016; Toydemir *et al*. 2017). However, due to limited budgets for short-span bridges, especially for those in rural areas, an economical, efficient and effective testing method is necessary for evaluation of their safety. Some attempts have been made to develop testing methods using mobile vehicles.

Pioneering work by Yang and Lin (2005) led to the identification of basic modal parameters from a moving vehicle's acceleration. A modified vehicle capable of producing an impact upon a bridge whilst simultaneously scanning for structural damage based on its reactions was developed by Xiang *et al.* (2005). Guo *et al*. (2009) evaluated bridge performance by establishing the relationship between a passing vehicle's reactions and structural damage. Though these methods were efficient, they were limited to the identification of basic modal parameters and preliminary damage.

As a kind of forced vibration test, the impact test, by measuring both input forces and output responses, has the merit to extract the Frequency Response Function (FRF) consistent with analytic solutions, including its shape and amplitude, while ambient vibration testing data is restricted to the shape of the structural FRF (i.e. it does not include amplitude). As a result, the impact test can be used to successfully identify not only basic modal parameters (frequencies, damping ratios and mode shapes) but also deep-level parameters, such as the scaling factor and flexibility matrix (Zhang *et al*. 2014).

Although impact tests have long been studied, they have not been widely used in engineering practices for the following reasons. First, it is not easy to excite a bridge because the energy generated by the available impacting equipment is limited. For example, a sledge hammer cannot fully excite the dynamic characteristics of a bridge because of its low impact force (less than 20kN). Despite Zhang and Moon (2012) and De Vitis *et al*. (2013) developed a drop-

*Corresponding author, Professor
E-mail: jian@seu.edu.cn

http://www.techno-press.com/journals/sem&subpage=7
ISSN: 1225-4568 (Print), 1598-6217 (Online)

weight exciter which could generate a 100kN impact force with a wide frequency band (0–200Hz), this excitation device was inefficient because it needed to be stopped when exciting the bridge. Second, the lack of a structural identification theory to impact testing discourages use of the method; such a theory must be based upon impact test data, and this work is still in progress. Brownjohn *et al*. (2007) performed bridge vibration tests using an exciter, but the impact force was not used in the data processing stage. Catbas *et al*. (2004) and Brown and Witter (2011) developed a flexibility identification theory by using impacting forces and structural responses, from which the structural deflection under any static load can be accurately predicted, and researchers applied it to several short-/middle-span bridges and proved that predicted deflections from the impact testing data were comparable with those from static truck load tests (Zhang and Moon 2012; Tian *et al*. 2017). A drawback to the traditional impact testing method is that it requires a large number of sensors deployed across the entire structure. To overcome this problem, the idea of subdividing the structure to be analyzed into smaller sub-structures was proposed: the test data from all sub-structures could then be integrated to allow the flexibility matrix of the entire structure to be identified. These proposals led to a series of algorithms including the multiple reference method (Zhang and Moon 2012), the single reference method (Zhang *et al*. 2014; Zhang *et al*. 2015) and the reference-free method (Guo *et al*. 2018). In order to improve the testing efficiency, Tian *et al*. (2019) proposed a mobile impact testing method with noncontact vision-based measurement to identify mode shapes and flexibility matrix of the entire structure. However, these test methods were not convenient because they all required an impact test to be performed on each sub-structure independently.

In order to make more improvement for the impact tests described above, we have developed a bridge testing method using continuous wheel forces excitation, and we put forward a corresponding structural flexibility identification theory. Our method utilizes a moving vehicle to continuously excite a bridge under conditions in which the wheel forces are measurable. By continuously instead of intermittently exciting the bridge, the proposed test is more efficient than a sledge-hammer test or a drop-weight test. However, current test data processing methods are no longer applicable because the vehicle–bridge interaction forces act on the continuous bridge space, whereas the traditional impacting forces from a hammer or a drop-weight exciter act on discrete bridge nodes. Thus, it is necessary to develop a new structural identification theory for our proposed test.

The article is set out as follows. In Section 2, we present the idea of bridge dynamic test excited by the continuous wheel forces. In Section 3, we derive the structural flexibility identification theory, which includes equivalent load distribution, the eFRFs construction and modal scaling factor identification. In Sections 4 to 6, we validate the effectiveness of our proposed method via experimental and numerical examples and a parametric analysis is further performed to investigate the robustness of the proposed method. Finally, in Section 7 we present our conclusions.

2. Bridge dynamic test using continuous force excitation

To improve the performance of conventional bridge SHM by a drop-weight impact test, here we propose a continuous wheel forces excited bridge dynamic test in which we regard a moving vehicle as a continuous hammer exciter that causes the vibration of a bridge. Apart from retaining the advantage of an impact test, i.e. both the input force and structural reactions are measurable, the proposed test is much easier to perform than the traditional impact test because a moving vehicle can excite the whole bridge without stopping while a traditional point-impact test has to be repeatedly stopped and exciters prepared. For detecting the wheel forces acting on a bridge in real time, the Wheel Force Transducer (Six Axis Wheel Force Transducer) designed by Michigan Scientific Corporation was installed on the vehicle; for detecting the response of the bridge, accelerometers were installed on the bridge. As shown in Fig. 1, the wheel forces and the acceleration of the bridge should enable the estimation of FRF of the bridge, because both input forces and output responses are measured. The FRF estimated from the force-controlled vibration test data will be exactly the same as the analytical data calculated from structural intrinsic parameters (mass, stiffness, etc.), from which structural dynamic characteristics (modal parameters) and static characteristics (flexibility) can be accurately identified; in comparison, data from ambient vibration tests can only generate the shape of the structural FRF (not the amplitude), from which only structural dynamic characteristics (modal parameters) can be identified (Zhang *et al*. 2014). The specific analysis is as follows.

The analytical form of a displacement FRF $H_{oi}(\omega)$ of a multiple Degree-of-Freedom (DOF) system is as follows when the Dirac force acting on the *i*th DOF and the displacement of the *o*th DOF are known:

$$H_{oi}(\omega) = \sum_{r=1}^{n} \frac{\phi_{or}\phi_{ir}}{M_r\omega_{dr}} \int_{-\infty}^{+\infty} exp\,(-\xi_r\omega_r t - j\omega t) sin\,(\omega_{dr} t) dt \tag{1}$$

where t is time; ω is frequency; ω_{dr} is the damped modal frequency of the *r*th modal order; ω_r is the modal frequency of the *r*th modal order; ϕ_{or} and ϕ_{ir} are the *r*th mode shape at the *o*th and the *i*th node, respectively; M_r is the modal mass of the *r*th modal order; ξ_r is the damping ratio of the *r*th modal order; and $j = \sqrt{-1}$.

The displacement FRF $H_{imp,oi}(\omega)$ from the force-controlled vibration test, where both the force $f_i(t)$ and the structural response $x_o(t)$ are measurable, is as follows:

$$H_{imp,oi}(\omega) = \frac{\sum_1^{N_{avg}} X_o\,(\omega) F_i^*(\omega)}{\sum_1^{N_{avg}} F_i\,(\omega) F_i^*(\omega)} = \sum_{r=1}^{n} \frac{\phi_{or}\phi_{ir}}{M_r\omega_{dr}} \int_{-\infty}^{+\infty} exp\,(-\xi_r\omega_r t - j\omega t) sin\,(\omega_{dr} t) dt \tag{2}$$

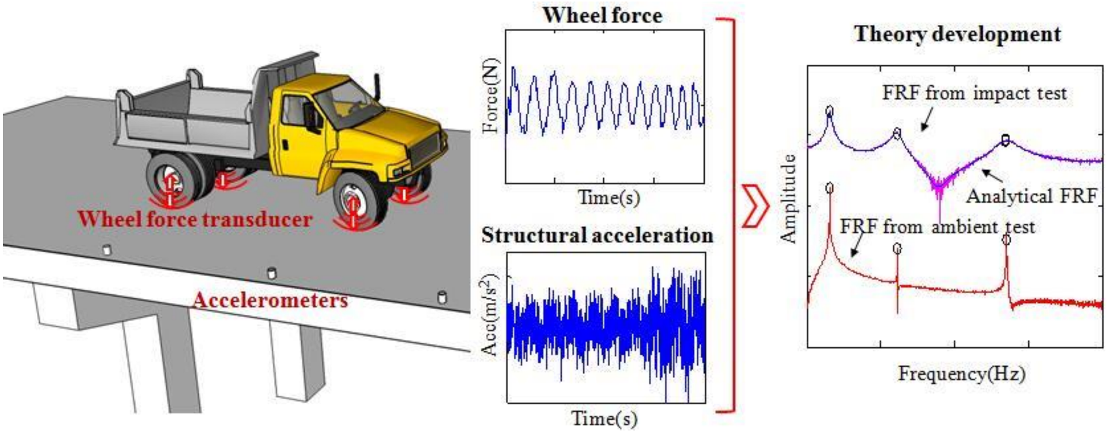

Fig. 1 Idea of bridge dynamic test induced by continuous wheel force excitation

where $F_i(\omega)$ is the Fourier Transform (FT) of the force $f_i(t)$; $F_i^*(\omega)$ is the complex conjugate of $F_i(\omega)$; $X_o(\omega)$ is the FT of the structural response $x_o(t)$; and N_{avg} is the number of the spectrum average ($N_{avg}=1$ in this derivation).

The displacement FRF $H_{amb,oi}(\omega)$ from an ambient test, where white-noise excitations $f_k(t)(k=1,2,\dots,m)$ on the kth DOF are assumed and only structural responses are measurable, is as follows using the Natural Excitation Technique (Zhang *et al*. 2014):

$$\begin{aligned} H_{amb,oi}(\omega) &= \int_{-\infty}^{+\infty} C_{oi}(\tau) exp\,(-j\omega\tau)\,d\tau \\ &= \sum_{r=1}^{n} \Im_{oi}^{r} \int_{-\infty}^{\infty} exp\,(-\xi_r\omega_r\tau \\ &\quad - j\omega\tau) sin\,(\omega_{dr}\tau+\theta_r)d\tau \end{aligned} \tag{3}$$

where $C_{oi}(\tau)=\sum_{r=1}^{n}\Im_{oi}^{r} exp\,(-\xi_r\omega_r\tau) sin\,(\omega_{dr}\tau+\theta_r)$ is the cross correlation of structural responses under all the white-noise excitations; τ is the cross correlation lag, $\Im_{oi}^{r}=\frac{\phi_{or}}{M_r\omega_{dr}}\sum_{s=1}^{n}\sum_{k=1}^{m}\frac{\Theta_k}{2}\frac{\phi_{kr}\phi_{is}\phi_{ks}}{M_s}[J_{rs}^2+I_{rs}^2]^{-\frac{1}{2}}$; Θ_k is the intensity of a white-noise excitation; ϕ_{kr} is the value of the rth mode shape at the kth DOF; ϕ_{is} and ϕ_{ks} are the values of the sth mode shape at the ith DOF and the kth DOF, respectively; M_s is the modal mass of the sth modal order; ω_{ds} is the damped modal frequency of the sth modal order; ω_s is the modal frequency of the sth modal order; ξ_s is the damping ratio of the sth modal order; $J_{rs}=(\omega_{ds}^2-\omega_{dr}^2)+(\xi_r\omega_r+\xi_s\omega_s)^2$; $I_{rs}=2\omega_{dr}(\xi_r\omega_r+\xi_s\omega_s)$; and $\theta_r=arctan\,(\frac{I_{rs}}{J_{rs}})$.

It should be noted that Eqs. (1)-(2) are equivalent, meaning that the force-controlled vibration test has the merit of extracting the analytical displacement FRF. In contrast, an ambient test can only extract a displacement FRF having a similar shape to the analytical FRF but with different amplitude as shown in Eqs. (1)-(3). The difference between FRFs from an impact test and an ambient test is more clearly illustrated in Fig. 1. Thus, the ambient test can only identify basic modal parameters such as frequencies, damping ratios and mode shapes. On the other hand, the force-controlled vibration test identifies not only the structural modal parameters but also more detailed structural parameters, in particular flexibility, which indicates the distribution of structural stiffness and which is very sensitive to structural damages. Furthermore, the structural flexibility can be used as an index for damage identification (Nobahari and Seyedpoor. 2013), performance evaluation and life-cycle prognosis.

Though the proposed test method shown in Fig. 1 is more convenient and efficient than the traditional impact tests, the structural identification theories accompanying to the latter cannot be directly applied to the proposed method, because a hammer or a drop weight has an impact across discrete structural nodes, whereas wheel forces (as proposed in our method) act on a continuous bridge space. We therefore have developed in this paper a novel structural identification theory to process the continuous wheel forces and extract structural dynamic characteristics (modal parameters) and static characteristics (flexibility).

3. The corresponding structural flexibility identification theory

The bridge excited by continuous wheel force is actually a time-variant vehicle–bridge coupling system, in which vehicle and bridge excite each other; because we mainly concentrate on the in-service conditions of bridges, we need to decouple the coupled system in order to obtain bridge parameters. In the coupling system, it is well known that vehicle and bridge are connected by wheels and they are excited to each other through vehicle–bridge interaction forces. Therefore, by measuring all wheel forces, the coupled system can be divided into two systems, i.e. the vehicle system and the bridge system, which have the common excitation source that is the interaction force. A Wheel Force Transducer, which can accurately measure all wheel forces of the vehicle, is commercially available and recommended.

3.1 Equivalent load distribution

Although the bridge dynamic test under continuous force is more convenient to perform than the sledge-

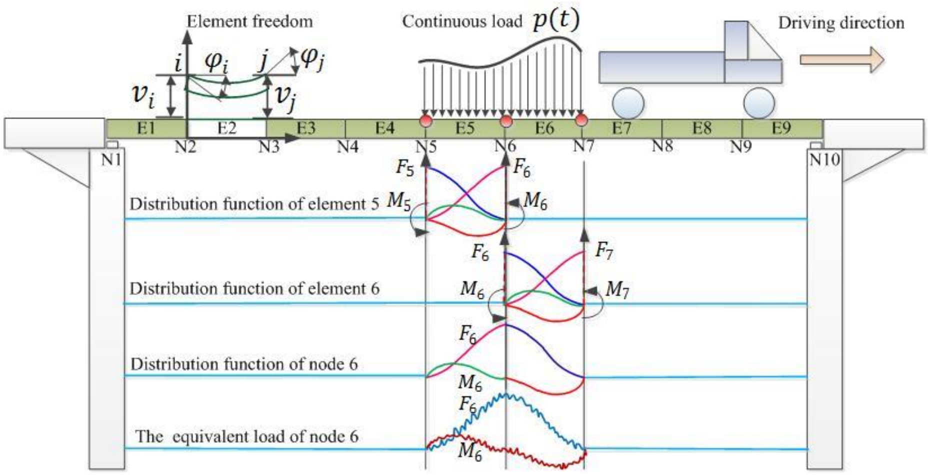

Fig. 2 Illustration of equivalent load distribution

hammer test or the drop-weight test, the theories supporting the latter only deal with excitation force acting on discrete nodes, and they are unsuitable in the case of wheel forces acting on a continuous space. Here, we transform continuous wheel forces into nodal forces using the equivalent load distribution.

The first step is to consider the accelerometer layout scheme. Experience of previous impact testing indicates that, in general, accelerometers can be uniformly distributed along two sides of a bridge deck. The distribution of the elements can also be made in accordance with the sensor distribution, an element being defined as the space between two adjacent sensors on the same side of the bridge deck. For the testing method proposed in this paper, sensors can be deployed non-uniformly as well. The position and length of elements are determined according to the location of sensors.

For a plane beam element, consisting of two nodes (*i* and *j*) and four DOFs $\{d\} = [v_i \ \varphi_i \ v_j \ \varphi_j]^T$, where v_i and v_j are the vertical displacements of the *i*th and the *j*th nodes, respectively; and φ_i and φ_j are the rotation angles of the *i*th and the *j*th nodes, respectively, as shown in Fig. 2. Assuming that the displacement distribution $v(x)$ of the element is a Hermite interpolation function:

$$N_v^e(x) = \left[1-\frac{3x^2}{l^2}+\frac{2x^3}{l^3} \quad -x+\frac{2x^2}{l}-\frac{x^3}{l^2} \quad \frac{3x^2}{l^2}-\frac{2x^3}{l^3} \quad \frac{x^2}{l}-\frac{x^3}{l^2}\right] \tag{4}$$

where l is the length of element.

The equivalent nodal loads F_E^e can be described using the distributed force $f^e(x)$ as follows:

$$F_E^{e^T} = \begin{Bmatrix} F_i \\ M_i \\ F_j \\ M_j \end{Bmatrix} = \int_0^l f^e(x) N_v^{e^T}(x)\mathrm{d}x \tag{5}$$

where F_i, F_j, M_i, M_j are equivalent nodal forces and moments. It is worth noting that the displacement distribution function $N_v^e(x)$ plays an important role for deriving the equivalent load distribution.

The second step is to extend the equivalent load distribution from an element to the whole bridge structure and taking the influence of time t into consideration. The equivalent nodal loads of a bridge having *n* nodes are:

$$F_E^{b^T}(t) = \begin{Bmatrix} F_1(t) \\ M_1(t) \\ F_2(t) \\ M_2(t) \\ \vdots \\ F_{n-1}(t) \\ M_{n-1}(t) \\ F_n(t) \\ M_n(t) \end{Bmatrix} = N_v^b(x)\{f^b(x,t)\}\Delta x$$

$$= \begin{bmatrix} N_1(x_1^{e1}) & \cdots & N_1(x_m^{e1}) & 0 & \cdots & 0 & \cdots & 0 & \cdots & 0 & 0 & \cdots & 0 \\ N_2(x_1^{e1}) & \cdots & N_2(x_m^{e1}) & 0 & \cdots & 0 & \cdots & 0 & \cdots & 0 & 0 & \cdots & 0 \\ N_3(x_1^{e1}) & \cdots & N_3(x_m^{e1}) & N_1(x_1^{e2}) & \cdots & N_1(x_m^{e2}) & \cdots & 0 & \cdots & 0 & 0 & \cdots & 0 \\ N_4(x_1^{e1}) & \cdots & N_4(x_m^{e1}) & N_2(x_1^{e2}) & \cdots & N_2(x_m^{e2}) & \cdots & 0 & \cdots & 0 & 0 & \cdots & 0 \\ \vdots & \vdots & \vdots & \vdots & \vdots & \vdots & \vdots & \vdots & \vdots & \vdots & \vdots & \vdots & \vdots \\ 0 & \cdots & 0 & 0 & \cdots & 0 & \cdots & N_3\left(x_1^{e(n-1)}\right) & \cdots & N_3\left(x_m^{e(n-1)}\right) & N_1(x_1^{en}) & \cdots & N_1(x_m^{en}) \\ 0 & \cdots & 0 & 0 & \cdots & 0 & \cdots & N_4\left(x_1^{e(n-1)}\right) & \cdots & N_4\left(x_m^{e(n-1)}\right) & N_2(x_1^{en}) & \cdots & N_2(x_m^{en}) \\ 0 & \cdots & 0 & 0 & \cdots & 0 & \cdots & 0 & \cdots & 0 & N_3(x_1^{en}) & \cdots & N_3(x_m^{en}) \\ 0 & \cdots & 0 & 0 & \cdots & 0 & \cdots & 0 & \cdots & 0 & N_4(x_1^{en}) & \cdots & N_4(x_1^{en}) \end{bmatrix} \begin{Bmatrix} f(x_1^{e1},t)\Delta x \\ \vdots \\ f(x_m^{e1},t)\Delta x \\ f(x_1^{e2},t)\Delta x \\ \vdots \\ f(x_m^{e2},t)\Delta x \\ \vdots \\ f(x_1^{e(n-1)},t)\Delta x \\ \vdots \\ f(x_m^{e(n-1)},t)\Delta x \\ f(x_1^{en},t)\Delta x \\ \vdots \\ f(x_m^{en},t)\Delta x \end{Bmatrix} \tag{6}$$

where $x_1^{e1} \cdots x_m^{e1}, x_1^{e2} \cdots x_m^{e2}, x_1^{e(n-1)} \cdots x_m^{e(n-1)}, x_1^{en} \cdots x_m^{en}$ are coordinates of the distributed force, the superscript representing the element and the subscript representing a specific position in the element; Δx is the distance between two continuous coordinates, assuming that all coordinates are uniformly distributed (though it is not necessary); and where $F_E^b(t)$, $N_v^b(x)$, $\{f^b(x,t)\}$ are equivalent nodal loads, the distribution function and the distributed force of the bridge, respectively. Obviously, the velocity of vehicle is feasible for either constant or variable cases. Note that for the proposed method, temporal and spatial information on various wheel forces is necessary when the vehicle runs over the bridge. Generally, the front axle and rear axle of the vehicle successively pass the same element. Thus, the force applied to this element is a superposition of front and rear axle wheel forces within temporal and spatial domains.

Now taking the simply supported beam in Fig. 2 as an example and considering the in-plane motion only. Though only the wheel forces $\{f^w(t)\}$ are measured directly in the rapid test, the vehicle speed is also recorded to help determining the distributed force $\{f^b(x,t)\}$. The whole beam is divided into nine elements labeled E1 to E9 and the nodes labeled N1 to N10. The first and the second rows in Fig. 2 illustrate the distribution functions of elements E5 and E6 respectively and the third row illustrates the distribution function of node N6. The fourth row displays the nodal loads of N6. Evidently, each node has two kinds of input: the equivalent vertical nodal force and equivalent nodal moment.

3.2 Scaling factor and flexibility identification

Once the continuous wheel forces are transformed into equivalent nodal loads, bridge is considered as a Multi-Input Multi-Output (MIMO) system, its acceleration FRFs can be estimated using equivalent nodal loads and structural accelerations. Next, the acceleration FRFs are converted into displacement FRFs, and they are used to identify structural basic modal parameters. It should be noted that each node has two inputs (the vertical force and the moment) and a single output signal (the acceleration). That is to say, if the bridge has N_{in} inputs and N_{out} outputs after load distribution, accordingly, the dimension of the FRF matrix will be $N_{out} \times N_{in}$. However, only the relationship between the vertical force and the acceleration is of interest here. Thus, the new FRF matrix $[H^*]$ that excludes the coefficients associated with nodal moment from the whole FRF matrix can be achieved by introducing a transformation matrix $[R]$:

$$[H^*]_{N_{out}\times N_{out}} = [H]_{N_{out}\times N_{in}}[R]_{N_{in}\times N_{out}} \tag{7}$$

where

$$[R]_{N_{in}\times N_{out}} = \begin{bmatrix} R_{1,1} & R_{1,2} & \cdots & R_{1,N_{out}} \\ R_{2,1} & R_{2,2} & \cdots & R_{2,N_{out}} \\ \vdots & \vdots & \ddots & \vdots \\ R_{N_{in},1} & R_{N_{in},2} & \cdots & R_{N_{in},N_{out}} \end{bmatrix},$$

$$R_{i,j} = \begin{cases} 1, & i = 2j-1 \\ 0, & i \neq 2j-1 \end{cases}$$

By performing the Singular Value Decomposition (SVD) on the new FRF matrix, the left singular matrix $[U(\omega)]$, the right singular matrix $[V(\omega)]$, and the singular value matrix $[S(\omega)]$, can be obtained. The FRF matrix can also be represented in terms of modal expansion through the superposition of individual modes. Both representations are described in Eq. (8). It can be seen that the matrix $[U(\omega)]$ corresponds to $[\Phi]$, the matrix $[S(\omega)]$ corresponds to $[\frac{1}{j\omega-\lambda_r}]$, and the matrix $[V(\omega)]$ corresponds to $[L]$:

$$[H^*] = [U(\omega)][S(\omega)][V(\omega)]^H = [\Phi][\frac{1}{j\omega - \lambda_r}][L]^T \tag{8}$$

where the superscript H denotes conjugate transposition, $[\Phi] = [\{\phi_1\}, \cdots, \{\phi_N\}, \{\phi_1^*\}, \cdots, \{\phi_N^*\}]$; $\{\phi_r\}$ is the r th mode shape; $\{\phi_r^*\}$ is the conjugate complex of $\{\phi_r\}$; λ_r is the system pole; $[L]$ is modal participation matrix in which $\{L_r\} = Q_r\{\phi_r\}$; Q_r is the modal scaling factor; and $\{\phi_r\}$ is the displacement mode shape. Natural frequencies and mode shapes are then identified by the Complex Mode Indicator Function (CMIF) method (Catbas *et al.* 2004).

Subsequently, eFRFs are constructed to improve the accuracy of the structural identification. The FRF is a superposition of modal parameters in frequency domain, in which the modal parameter identification of a single FRF will be affected by the coupling between different modes. Even if advanced algorithms can solve the modal coupling problem, a new problem is likely to appear, which is that modal parameters identified by different single mode FRFs cannot be identical due to the noise and the modal node. Therefore, in order to identify modal parameters more stably (such as system poles, damping ratios and modal scaling factors), it is necessary to reduce the multi-mode FRF to single mode FRFs in the frequency domain. The complex problem of the multi-dimensional modal coupling is transformed into a simple problem having only a single mode FRF, i.e. the eFRF:

$$eH(\omega)_r = \{u_r\}^T\{\phi_r\}\frac{Q_r}{j\omega - \lambda_r}\{\phi_r\}^T\{u_r\} \tag{9}$$

where r represents the rth modal order; $eH(\omega)_r$ is the eFRF; and $\{u_r\}$ is the first left singular vector.

The key issue in identifying the flexibility matrix is to identify the modal scaling factors. By using a polynomial fitting algorithm to fit the eFRF, the modal scaling factor Q_r can be calculated as

$$\frac{1}{Q_r} = \{u_r\}^T\{\phi_r\}\{\phi_r\}^T\{u_r\}\begin{Bmatrix} eH(\omega_1)_r \\ eH(\omega_2)_r \\ \vdots \\ eH(\omega_k)_r \end{Bmatrix}^+ \begin{Bmatrix} 1/(j\omega_1 - \lambda_r) \\ 1/(j\omega_2 - \lambda_r) \\ \vdots \\ 1/(j\omega_k - \lambda_r) \end{Bmatrix} \tag{10}$$

Having obtained the displacement mode shapes, system poles and scaling factors from all necessary modal orders ($r = 1, \ldots N$), the flexibility matrix of the structure can be identified by

$$Flex^d = \sum_{r=1}^{N}(\frac{Q_r\{\phi_r\}\{\phi_r\}^T}{-\lambda_r} + \frac{Q_r^*\{\phi_r^*\}\{\phi_r^*\}^T}{-\lambda_r^*}) \tag{11}$$

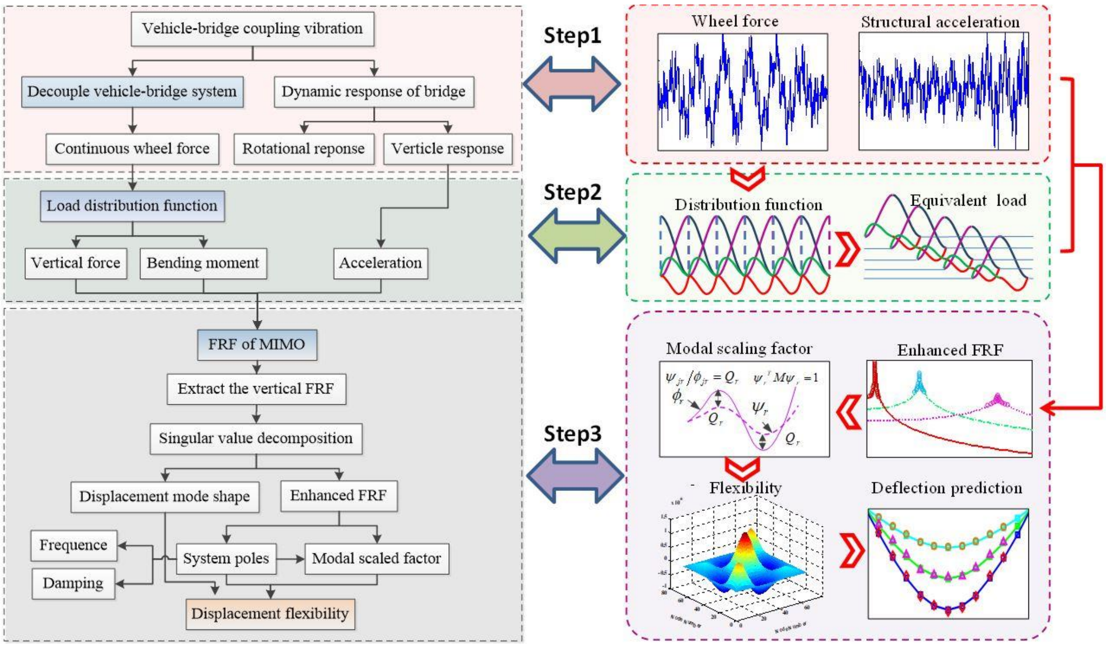

Fig. 3 Flowchart of the proposed method

where * represents the complex conjugate operation. It can be seen that the displacement flexibility matrix is the superposition of the modal parameters in the complex mode. The flexibility indicates the stiffness distribution of the structure. Assuming that a static force vector acting on the structure is $\{f_{static}\}$, then the static deflection of the structure can be predicted by $D = Flex^d\{f_{static}\}$.

3.3 Procedure of the proposed method

Based on the theoretical work developed above, Fig. 3 presents the framework of using continuous wheel forces to develop the bridge-testing methodology. First, the vehicle–bridge vertical interaction force is obtained by the Wheel Force Transducer. Second, the continuous interaction forces are transformed to the equivalent point-type forces by virtue of the calculated load distribution function. Third, combining the acquired acceleration response from the SHM system and the transformed input forces, the FRF of the structure is estimated. Finally, modal scaling factors and the flexibility matrix are identified by employing available modal identification algorithms. The identified flexibility matrix can be used to assess bridge performance. The details are as follows.

Step 1: Vehicle–bridge coupling system decoupling. The bridge is excited by the moving vehicle, and simultaneously all wheel forces and the acceleration of the bridge are measured.

Step 2: Equivalent nodal load generation. First, the elements are generated according to the deployed accelerometers by using two adjacent sensors to determine an element at the same side of the bridge deck. Second, all the measured wheel forces are distributed to all nodes via Eq. (6). This process results in each node having two kinds of input, the equivalent vertical nodal force and equivalent nodal moment, while the output at each node is only the vertical acceleration.

Step 3: Displacement flexibility matrix identification. First, the displacement FRF is estimated from the input and output data. Note that this FRF is the dimension of $N_{out} \times N_{in}$ because of the existence of nodal moment. This FRF is further reduced to the dimension of $N_{in} \times N_{in}$ via Eq. (7) to eliminate the angular DOF. Second, a SVD is performed for the reduced FRF to obtain CMIF curves via Eq. (8) and eFRF via Eq. (9), and structural frequencies, damping ratios and mode shapes are identified from Eq. (8). Finally, the modal scaling factor can be solved from the least squares estimation formulation from Eq. (10) and the flexibility matrix can be identified from Eq. (11).

4. Laboratory experiment example

4.1 Experimental design and monitoring strategy

In order to verify the proposed methodology, a laboratory experiment was conducted in which a loaded tire moving over a simply supported beam was investigated, and real-time measurements included the wheel force and vertical accelerations of a simple beam. Static load tests were then conducted by applying mass blocks, and vertical displacements of the simple beam were measured. The wheel force and accelerations were used to identify those structural parameters and static displacements that were necessary to verify the predicted deflection by the identified structural flexibility.

The structure to be studied was a simply supported beam with a length of 5868mm as shown in Fig. 4(a). It was a hot-rolled channel-section steel beam made of Chinese standard steel material Q235. The beam was divided into twelve elements (E1–E12) and thirteen nodes (N1–N13) as shown in Fig. 4(c). The monitoring system of the beam comprised of eleven accelerometers (type: ICP 393B04) and eleven cable-extension displacement transducers (type:

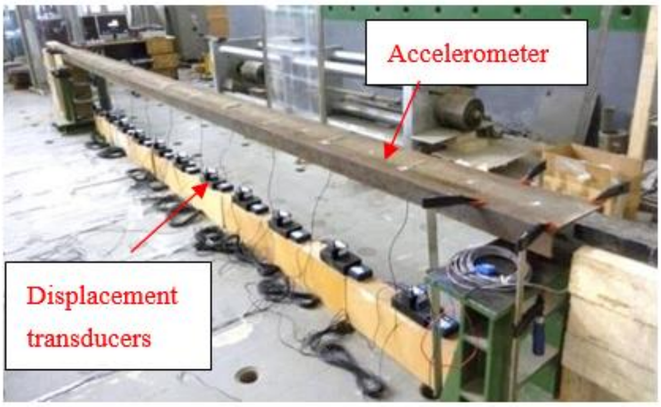

(a) Beam

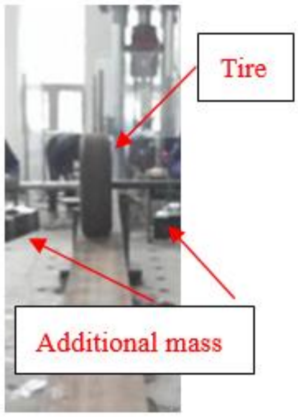

(b) Tire-Beam-Interaction

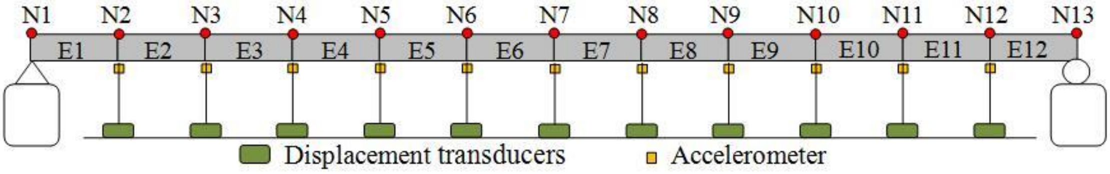

(c) Monitoring strategy of the beam

Fig. 4 Experiment design

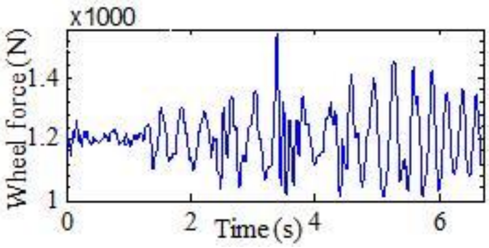

(a) Wheel force

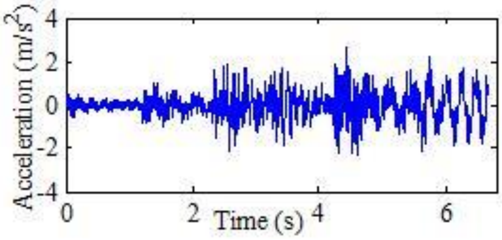

(b) A typical nodal acceleration

Fig. 5 Experiment data

CELESCO PT1DC). Accelerometers and displacement transducers dynamically measured the vertical deformation of the beam's central axis from nodes N2 to N12. The single tire (type: Giti Wingro 165/70R13) was adopted to simulate the tire force on the beam structure as shown in Fig. 4(b). An axle through the center of the tire served as a bar for propulsion, and additional masses were hung on the bar symmetrically for serving as the vehicle weight. Wheel force monitoring system was installed on tires to obtain continuous wheel force.

4.2 Description of the experiment

Two kinds of tests were conducted: the first was a tire–beam interaction experiment to identify the beam parameters, and the second was a static load experiment to verify the reliability of the identified flexibility. The experiment was conducted by rolling the loaded tire along the beam at a speed of 0.88m/s; the total mass of the tire including the additional mass was 120kg. Strip-shaped magnets were placed on the steel beam to mimic surface obstacles. The wheel force monitored by the wheel force monitoring system is shown in Fig. 5(a). Vertical beam accelerations (Fig. 5(b) displays a typical measurement) were combined with the wheel force to calculate the structural parameters. In order to verify the reliability of the identified parameters, namely the flexibility and basic modal parameters, static load tests were conducted by applying mass blocks at specified nodes on the simply supported beam, and its static deflections were measured by displacement transducers. Two static load cases were conducted: Case 1, three mass blocks weighing 30kg were placed on both nodes N5 and N9 respectively; and case 2, two mass blocks weighing 30kg were placed on each nodes N3, N4, N6, N8 and N11 respectively.

4.3 Structural identification results

The equivalent nodal loads of the simply supported beam were firstly calculated. As the simple beam was divided into twelve elements, the length of each element was, on average, 489mm. Based on Eqs. (4)-(6), the equivalent loads of each node were obtained and are shown in Fig. 6.

The simply supported beam was regarded as a MIMO system, consisting of 26 inputs (thirteen vertical forces and thirteen bending moments) and eleven outputs (vertical accelerations). The FRF representing the relationship between vertical forces and vertical accelerations was a 11×11 matrix obtained via Eq. (7). By performing the SVD of the FRF, a CMIF plot was drawn (Fig. 7(a)). It was determined by the reference nodes. For instance, should be

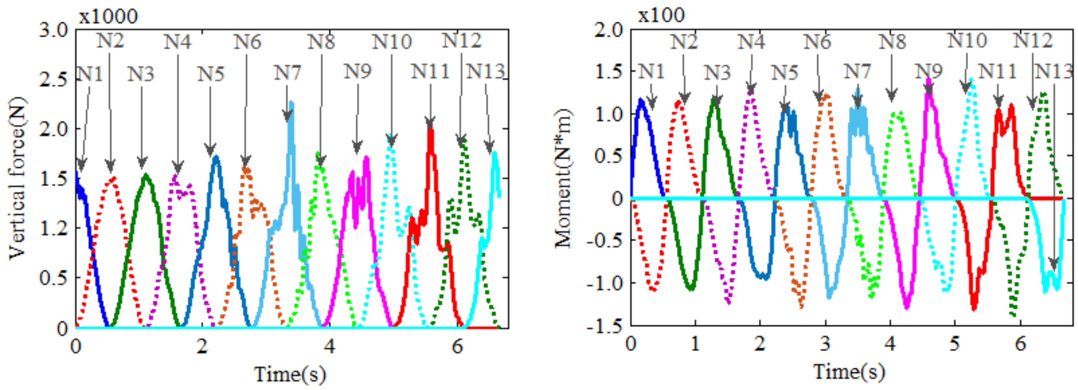

(a) Vertical forces (b) Moment

Fig. 6 Equivalent nodal loads

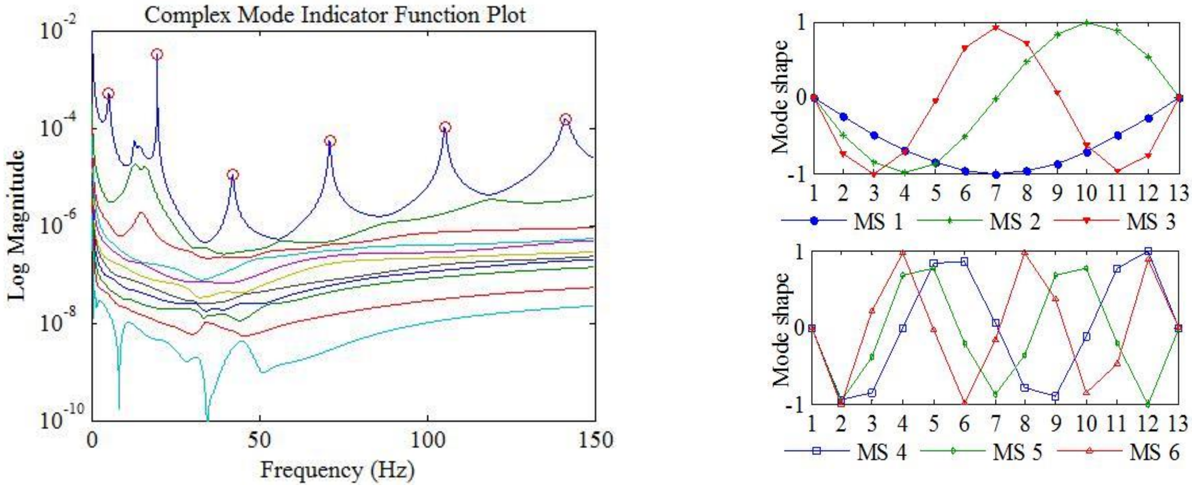

(a) CMIF plot (b) Mode shapes

Fig. 7 Identified results

noted that the number of curves in the CMIF plot there are thirteen curves in Fig. 7(a), because there are thirteen equivalent impacting nodes in the test. Natural frequencies were identified from CMIF peaks as denoted by the red circles in Fig. 7(a). The abscissa of the red dot in the figure is the structural nature frequency and the identified natural frequencies of the first six modes were 4.78, 18.89, 41.49, 71.52, 106.19, 142.18 (Hz), and the corresponding damping ratios were 4.44, 0.05, 0.82, 0.33, 0.34, 0.71(%). The mode shapes and the modal participation factor matrices were identified via Eq. (8), and the identified mode shapes (MS) are shown in Fig. 7(b), so that the eFRF could be constructed with Eq. (9), which was then used to identify the modal scaling factor.

The modal scaling factor was identified via Eq. (10). The structural flexibility matrix of the beam was then identified via Eq. (11), and structural deflections under any static load could be predicted. Static loads for the two cases were used to verify the effectiveness of the identified flexibility. For instance, the predicted deflection under the static loads in Case 1 (i.e. 882N, 882N at nodes N5, N9 respectively) are shown in Fig. 8(a), and the predicted deflection under the static loads in Case 2 (i.e. 588N, 588N, 588N, 588N, 588N at nodes N3, N4, N6, N8, N11 respectively) are shown in Fig. 8(b). In both predictions, curves denoted by '3 modes' means that the flexibility was calculated from the modal parameters of the first three modes. It is seen from Eq. (11) that the flexibility has been estimated as the sum of the residuals normalized by the eigenvalues and their conjugate in all identified structural modes. As illustrated by Fig. 8, the simplicity of this structure meant that the flexibility calculated using only the first mode could accurately capture the real structural characteristics, which is reasonable from our knowledge of basic structural dynamics.

5. Numerical studies of a three-span continuous beam bridge

To verify the proposed structural identification theory under a more realistic level, a 2D model of the double-axle vehicle and a continuous bridge model were established in MATLAB. The vehicle with four DOF is shown in Fig. 9, it consists of ups and downs of freedom, nodal degree of freedom, with the front and back wheel set having a vertical displacement DOF. The vehicle was driven at a constant speed of 8m/s (28.8km/h). The bridge with a double cell section was modelled as a continuous bridge using Euler-Bernoulli beam theory and divided into eighteen elements and nineteen nodes from N1 to N19. Each node had two DOFs, i.e. the vertical displacement and the rotational

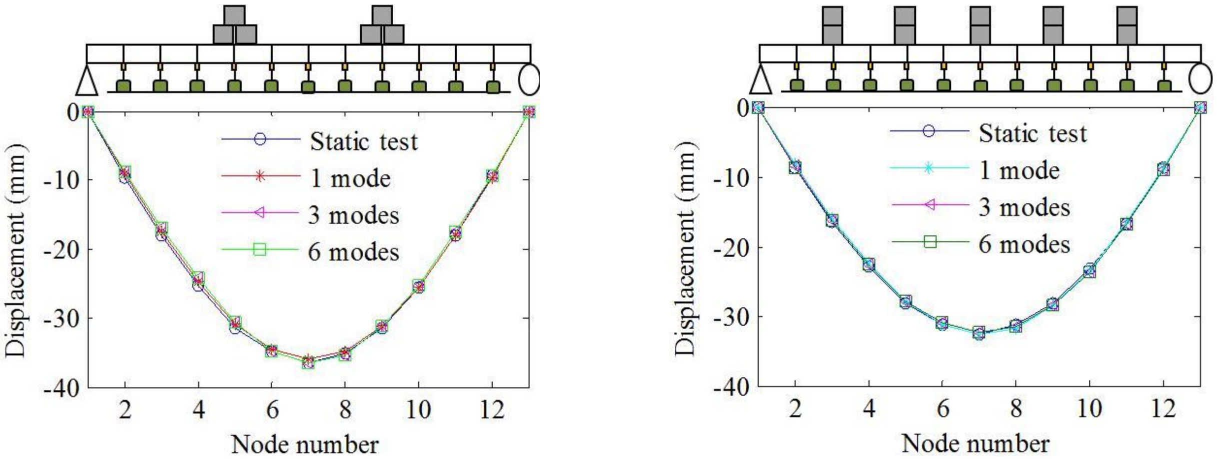

(a) Case 1 (b) Case 2

Fig. 8 Deflections prediction

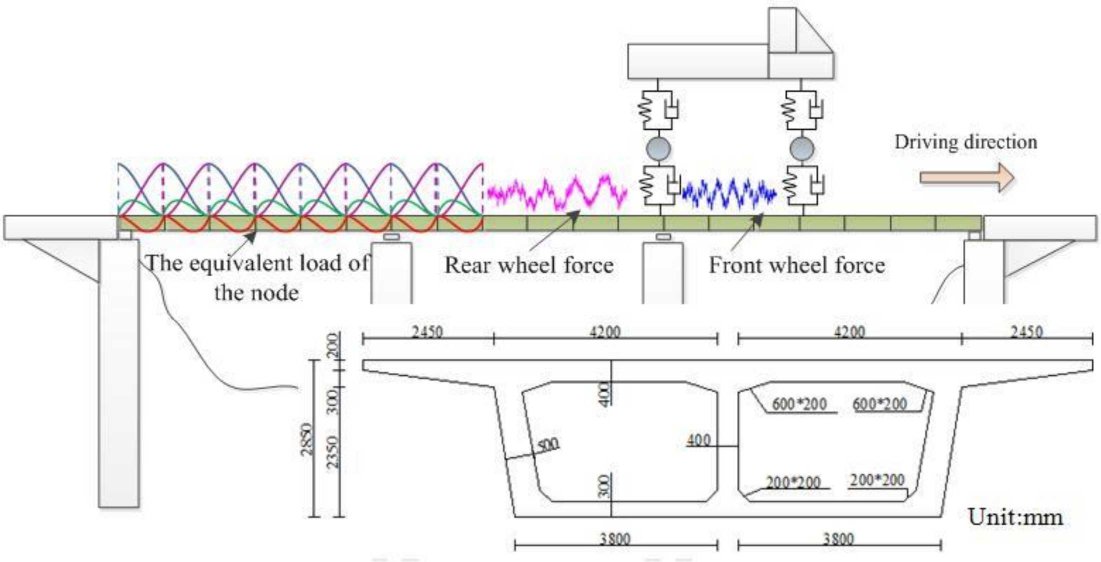

Fig. 9 Numerical simulation

angle, and the boundary conditions of continuous bridge were set by restraining the vertical degrees of freedom of the nodes at the supports. The Rayleigh damping was considered and the road surface roughness was simulated by the power spectral density (PSD) (Dodds and Robson. 1973) provided by International Organization for Standardization (ISO, 2016).

A road surface profile is usually assumed to be a zero-mean stationary Gaussian random process and can be generated through an inverse Fourier transformation (Deng and Cai. 2009) as:

$$r(X) = \sum_{k=1}^{N} \sqrt{2G(n_k)\Delta n} cos\,(2\pi n_k X + \theta_k) \tag{12}$$

where θ_k is the random phase angle uniformly distributed from 0 to 2 π; $G()$ and n_k are the PSD function (m^3/cycle) and the wave number (cycle/m), respectively. In this study, the PSD function was used:

$$G(n) = G(n_0)(\frac{n}{n_0})^{-2} \qquad (n_1 < n < n_2) \tag{13}$$

where n_0 is the discontinuity frequency of $1/2\pi$ (cycle/m); n is the spatial frequency (cycle/m); $G(n_0)$ is the roughness coefficient (m^3/cycle) whose classification index is from A (very good) to H (very poor); and n_1 and n_2 are the lower and upper cut-off frequencies, respectively. In this numerical simulation, the road surface roughness of "Level B" was used. Parameter settings of the vehicle and the bridge are listed in Table 1 and Fig. 9, and were used to solve the vehicle bridge coupling equation with the $Newmark - \beta$ method.

The front wheel force F_f and the rear wheel force F_r were calculated via the following equations:

$$F_f = \left(m_s \frac{a_2}{a_1 + a_2} + m_{t1}\right) g + m_{t1}\ddot{y}_{t1} + \frac{a_2}{a_1 + a_2} m_s \ddot{y}_s + \frac{1}{a_1 + a_2} J\ddot{\theta} \tag{14}$$

$$F_r = \left(m_s \frac{a_1}{a_1 + a_2} + m_{t2}\right) g + m_{t2}\ddot{y}_{t2} + \frac{a_1}{a_1 + a_2} m_s \ddot{y}_s - \frac{1}{a_1 + a_2} J\ddot{\theta} \tag{15}$$

Table 1 Bridge parameters and vehicle parameters

	Items	Parameters	Values
Bridge	Young's modulus of the bridge	E	$3.5 \times 10^{10} Pa$
	Moment of inertia of cross-section	I	$8.65\ kg\ m^2$
	Mass of the bridge per unit length	m	$3.6 \times 10^4 kg$
	The length of the bridge	L	3@20m
	The width of the bridge	W	13.3 m
Vehicle	The mass of the body	m_s	41750 kg
	Pitching moment of inertia of body	J	$2.08 \times 10^6 kg\ m^2$
	Mass of the front axle suspension	m_{t1}	$3.04 \times 10^3 kg$
	Mass of the rear axle suspension	m_{t1}	$3.04 \times 10^3 kg$
	Upper spring stiffness of the front axle	k_{s1}	$5.3 \times 10^5 N/m$
	Upper spring stiffness of the rear axle	k_{s2}	$5.3 \times 10^5 N/m$
	Upper damping of the front axle	c_{s1}	$9.02 \times 10^4 kg/s$
	Upper damping of the rear axle	c_{s2}	$9.02 \times 10^4 kg/s$
	Lower spring stiffness of the front axle	k_{t1}	$1.18 \times 10^6 N/m$
	Lower spring stiffness of the rear axle	k_{t2}	$1.18 \times 10^6 N/m$
	Lower damping of the front axle	c_{t1}	$3.92 \times 10^4 kg/s$
	Lower damping of the rear axle	c_{t2}	$3.92 \times 10^4 kg/s$
	Distance from center to front axle	a_1	2.75 m
	Distance from center to rear axle	a_2	2.75 m
	The total length of the vehicle	a	5.50 m
	The velocity of the vehicle	V	8.0 m/s

where $\ddot{y}_{t1}$ and $\ddot{y}_{t2}$ are the accelerations of the m_{t1} and m_{t2}, respectively; $\ddot{y}_s$ is the acceleration of the m_s; $\ddot{\theta}$ is the angle acceleration of the vehicle body; and g is the acceleration due to gravity. The calculated wheel forces are shown in Fig. 10(a), and a typical node acceleration of the bridge is shown in Fig. 10(b).

Equivalent nodal loads were then calculated. First, we substituted the element length $l = 3.33$m into Eq. (4) to obtain the distribution function of each element. Second, we constructed the distribution function of the whole bridge. Third, we calculated the equivalent nodal loads using Eq. (6). The equivalent loads of some nodes are shown in Fig. 11.

The FRF was estimated using equivalent nodal loads and accelerations. White noise of 5%, which is the ratio to the standard deviation of the simulated data, was added into all wheel forces and structural responses as the environmental noise. It was noticed that the dimension of the FRF was 19×38 because the bridge is a MIMO system of 38 inputs and 19 outputs. The required FRF matrix (representing the relationship between vertical forces and vertical accelerations) was then extracted from the original FRF matrix. The dimension of the new FRF calculated via Eq. (7) matrix was 19×19. By performing the SVD for the new FRF, the left singular matrix, the singular value matrix and the right singular matrix were obtained. The eFRF was estimated via Eq. (9) and the basic modal parameters shown in Table 2 were obtained. It is seen from Table 2 that the identified frequencies and damping ratios are very close to the theoretical values. The mode shapes and the modal participation factor matrices had been identified from the CMIF method via Eq. (10). Modal Assurance Criteria (MAC) values of mode shapes from the proposed method and the theoretical solutions are shown in Fig. 12(a). The minimum MAC value is 0.996, which illustrates that the identified modal shapes generated from the proposed methods are accurate. The structural flexibility matrix of the bridge structure was then identified via Eq. (11) as shown in Fig. 12(b).

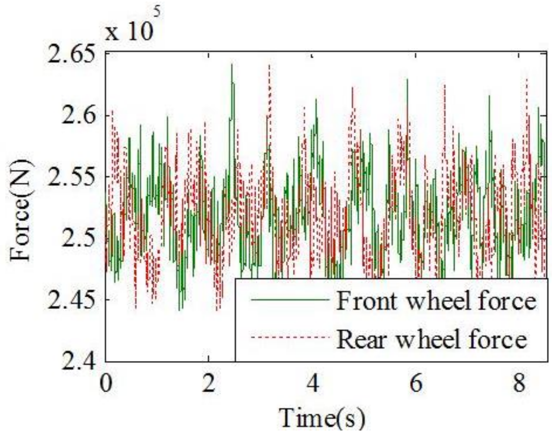

(a) Wheel forces

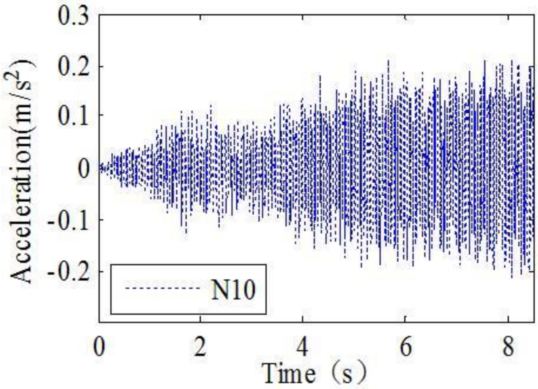

(b) A typical nodal acceleration

Fig. 10 Numerical simulation data

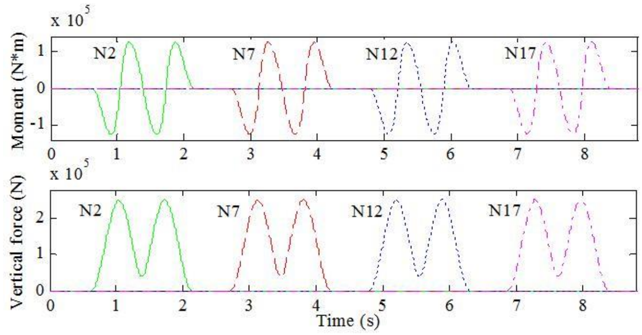

(a)Moments; (b) Vertical forces

Fig. 11 Equivalent loads of some nodes

Table 2 Identified results and theoretical values

Mode number	Theoretical frequency (Hz)	Identified frequency (Hz)	Frequency Error (%)	Theoretical damping ratio	Identified damping ratio	Damping ratio error (%)
1	11.39	11.38	0.10	0.07	0.07	0.20
2	14.60	14.57	0.16	0.07	0.07	0.27
3	21.31	21.24	0.33	0.09	0.09	0.58
4	45.60	44.91	1.50	0.15	0.15	2.91
5	51.97	50.97	1.93	0.17	0.16	3.77
6	63.79	61.97	2.86	0.21	0.20	5.41

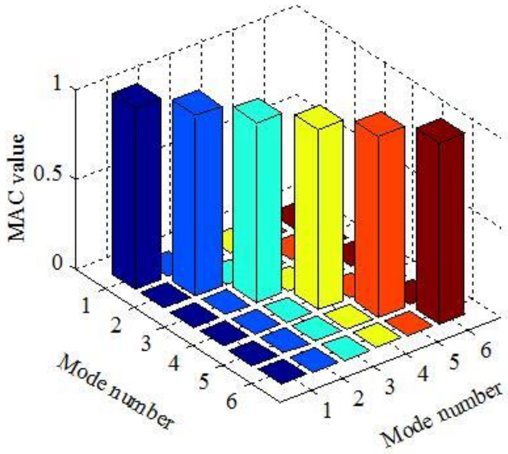

(a) MAC values

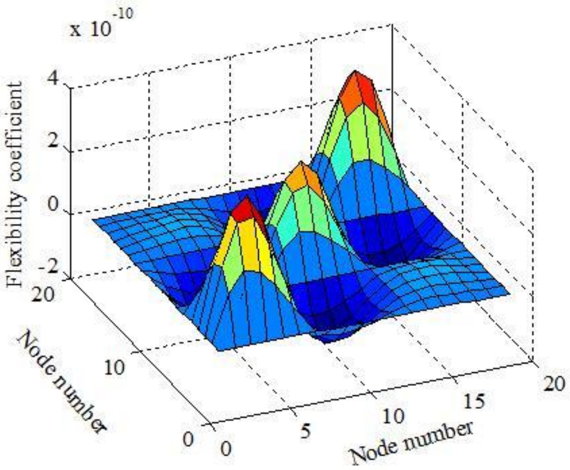

(b) Flexibility

Fig.12 Identified results

Once the structural flexibility is identified, deflection of the structure under any static load can be predicted. The predicted and actual deflections under three different static loads are shown in Fig. 13. In Case 1, static loads of 50kN were imposed on each node of N3, N8 and N13. In Case 2, static loads of 50kN were imposed on each node of N8 and N10. In Case 3, static loads of 20kN, 50kN and 20kN were imposed on nodes N4, N9 and N16, respectively. All three cases certify that the proposed method generates accurate identification results. In Case 3, further study was undertaken to determine how the mode number affects the accuracy of the deflection prediction. Eq. (11) shows that the flexibility is estimated as the sum of the residuals normalized by the eigenvalues and its conjugate in all identified structural modes. The error due to the mode number truncation in this case is shown in Fig. 13(c), where the curve denoted by ‘2 modes’ means that the corresponding flexibility was calculated from the modal parameters of the first two modes. It is seen that the flexibility using only the first two modes could not accurately capture the structural characteristics, whereas results from the first five modes were very close to the theoretical value; in this case, the modes after five orders did not contribute much to the structural flexibility calculation.

6. Parametric analysis

In Section 5 we presented the displacement flexibility identification and displacement prediction of a three-span continuous bridge. In this section we consider the effect of road roughness, vehicle speed, measurement noise, vehicle weight, vehicle’s stiffness and damping on displacement flexibility identification by a simulated static load experiment that enables the predicted displacement and theoretical displacement for each span to be compared. The predicted displacement is calculated from the flexibility obtained in this paper, and the theoretical displacement of the finite element simulation is calculated from the theoretical stiffness of the bridge. As shown in Fig. 14, static loaded trucks are distributed at the middle position of each span. The relative error is calculated by comparing the predicted displacement and theoretically calculated displacement at the position of the red dots in the spans.

6.1 Road roughness

First, we investigated the effect of road roughness on the identified flexibility. According to ISO-8608 specification, road roughness is classified into eight levels from “Level A” (very good) to “Level H” (very poor). In this study, six road roughness classes, i.e. A, B, C, D, E and F, based on the different values of PSD, were selected to investigate the effect of the road surface condition on the proposed method. In the calculation, the speed is set to 28.8km/h; the measurement noise is set to 0%; the vehicle weight is set to 41750kg; the different road roughness functions are added to the vehicle–bridge interaction analysis code, and the other parameters used are shown in Table 1. The relative errors between predicted displacement and theoretically calculated displacement with different road surface roughness are shown in Fig. 15(a); it can be seen that the maximum error for all types of road roughness is less than 0.49%, which demonstrates that road roughness has no influence on the flexibility identification.

6.2 Vehicle speed

Second, we investigated the effect of vehicle speed on flexibility identification. In the calculation, the roughness of the pavement is set to “Level A”; the measurement noise is set to 0%; the weight of the vehicle is set to 41750kg; Five

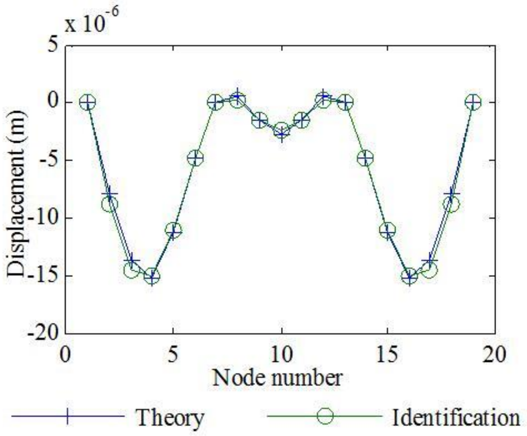

(a) Case 1

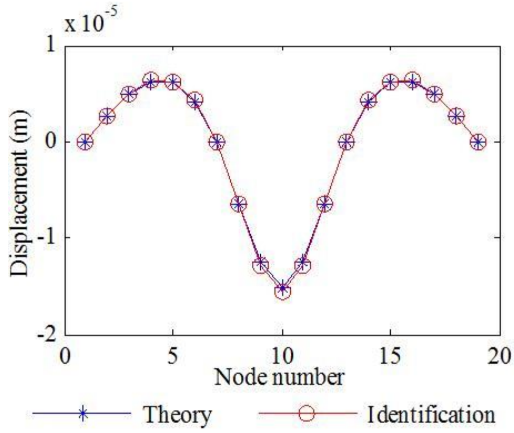

(b) Case 2

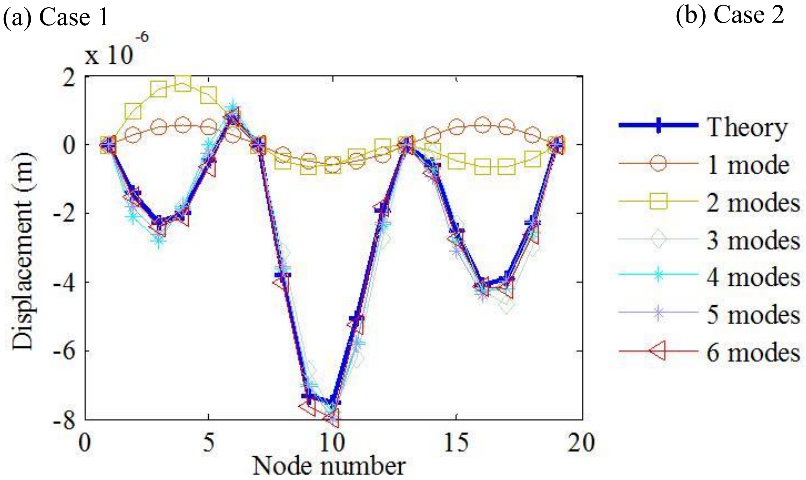

(c) Case 3

Fig. 13 Static deflection prediction

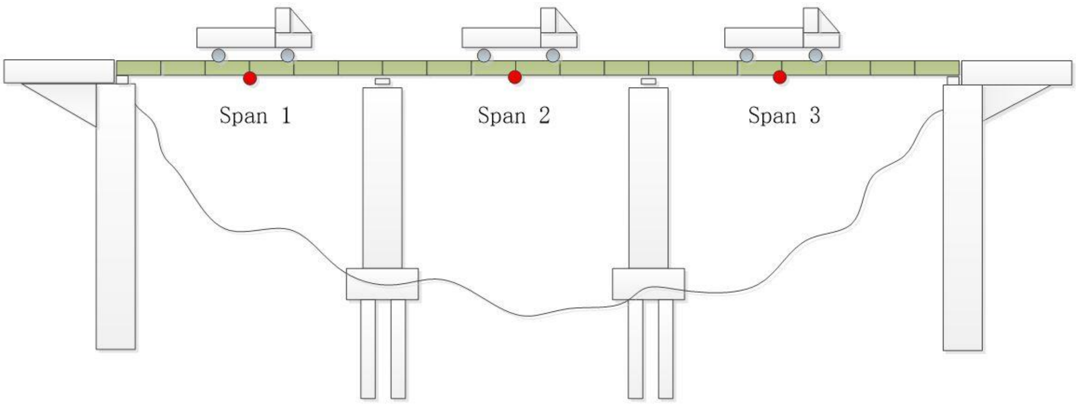

Fig.14 Static load experiment simulation

different vehicle speeds, $10, 20, 30, 40, 50\ km/h$, were studied and the other parameters used are shown in Table 1. The relative errors between predicted and theoretically calculated displacement with different vehicle speeds are shown in Fig. 15(b); it can be seen that the maximum error for any vehicle speed is less than 0.83%, which demonstrates that vehicle speed has no influence on the flexibility identification.

6.3 Measurement noise

Third, we studied the effect of measurement noise on flexibility identification in order to verify the robustness of the proposed method. In this numerical calculation, the road roughness is set to “Level A”; the vehicle speed is set to 28.8km/h; the vehicle weight is set to 41750kg; five cases of measurement noise at 0 %, 3%, 5%, 8%, 10% are considered, and the other parameters used are shown in Table 1. The relative errors between predicted and theoretically calculated displacement with different measurement noise are shown in Fig. 15(c); it can be seen that the relative errors increase with measurement noise but they are below 4.5%, which satisfies the precision requirement of practical engineering and proves the

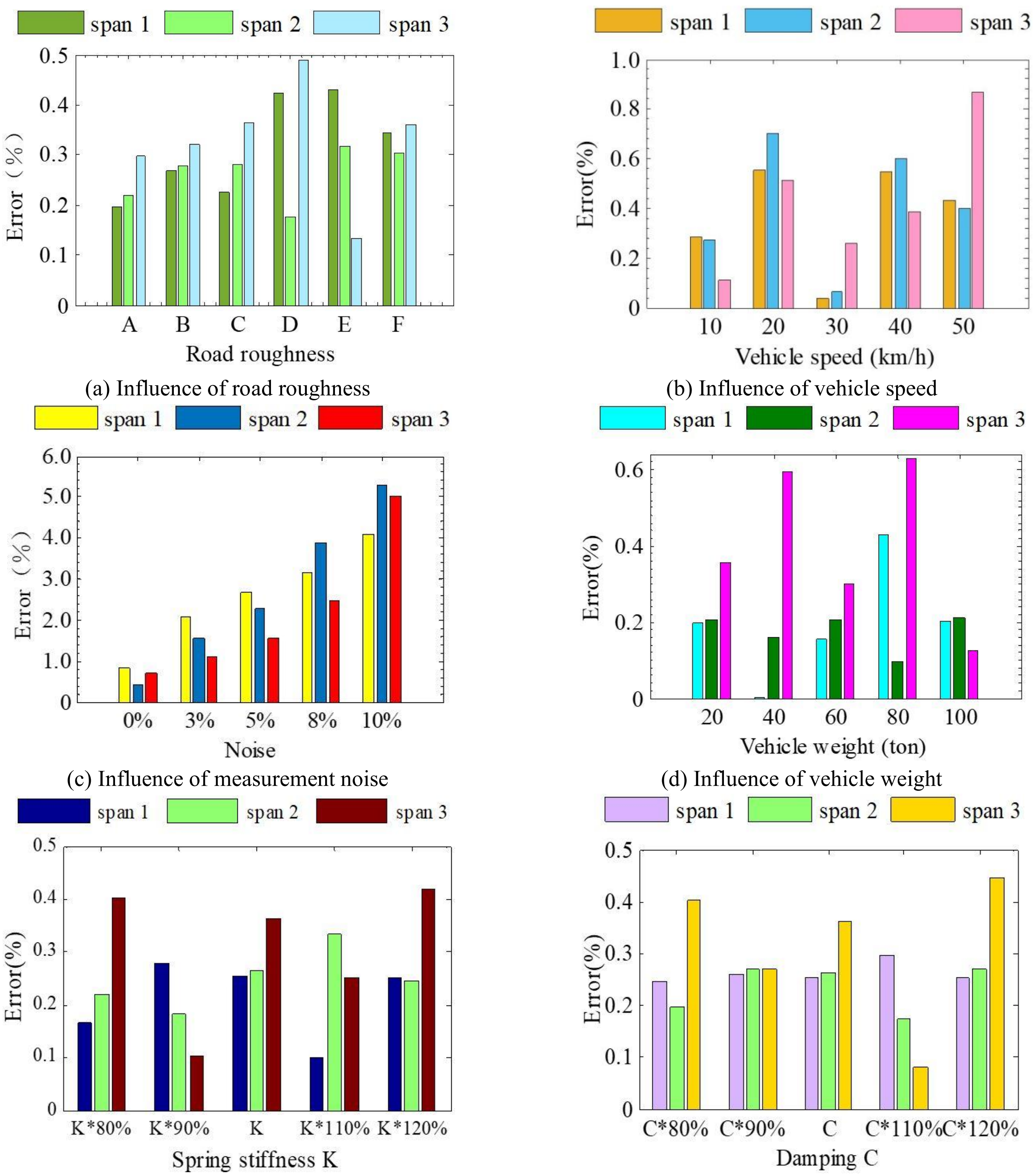

(a) Influence of road roughness

(b) Influence of vehicle speed

(c) Influence of measurement noise

(d) Influence of vehicle weight

(e) Influence of spring stiffness of vehicle

(f) Influence of damping of vehicle

Fig.15 Influence of various parameters on the error.

proposed method is robust in terms of noise. If the measurement noise affects the authenticity and stability of the data, signal pre-processing is a necessary means such as eliminating trend terms, band pass or wavelet filtering, applying window functions, etc.

6.4 Vehicle weight

Fourth, we studied the effect of vehicle weight on flexibility identification. In this numerical model, the road roughness is set to “Level A”; the speed is set to 28.8km/h; the measurement noise is 0%; five cases of vehicle weight of 20,40,60,80,100 ton are considered, and the other parameters used are shown in Table 1. The relative errors between predicted and theoretical displacement with different vehicle weight are shown in Fig. 15(d). It can be seen that the maximum error of all cases of vehicle weight is less than 0.62%, which demonstrates that the vehicle weight has little influence on flexibility identification.

6.5 Spring stiffness of vehicle

Fifth, we further studied the effect of spring stiffness K of vehicle on flexibility identification, where the K includes k_{s1}, k_{s2}, k_{t1}, k_{t2} listed in Table 1 are considered. In this numerical model, the road roughness is set to "Level A"; the speed is set to 28.8km/h; the measurement noise is 0%; the vehicle weight is set to 41750kg; five cases of spring stiffness of the vehicle with stiffness reduction of 20 %, 10 %, original stiffness, and stiffness increase of 10%, 20% are considered and the other parameters used are shown in Table 1. The relative errors of displacement between predicted and calculated theoretically with different spring stiffness of vehicle are shown in Fig. 15(e); it can be seen that the maximum error among all cases is less than 0.42%, which demonstrates that the spring stiffness of testing vehicle has little influence on flexibility identification.

6.6 Damping of vehicle

Sixth, we also studied the effect of damping C of vehicle on flexibility identification, where the C includes c_{s1}, c_{s2}, c_{t1}, c_{t2} as shown in Table 1 are considered. In this numerical model, the road roughness is set to "Level A"; the speed is set to 28.8km/h; the measurement noise is 0%; the vehicle weight is set to 41750kg; five cases of damping of vehicle with damping reduction of 20 %, 10 %, original damping, and damping increase of 10%, 20% are considered and the other parameters used are also shown in Table 1. The relative errors of displacement between predicted and calculated theoretically with different damping of vehicle are shown in Fig. 15(f); it can be seen that the maximum error among all cases is less than 0.45%, which demonstrates that the damping of testing vehicle has little influence on flexibility identification.

7. Conclusion

To improve the efficiency of impact vibration testing, a new bridge testing method with corresponding theory is proposed in this article. Specific conclusions are drawn as follows:

- The proposed method uses a moving vehicle instead of a hammer or artificial excitation device to excite a bridge without testing interruption, in which the wheel force (input) of the moving vehicle and acceleration responses (output) of the bridge are simultaneously measured for following structural identification.
- A deep-level parameters (i.e. scaling factor and flexibility matrix) identification method adapting to the new rapid testing method is proposed. It includes equivalent load distribution, eFRFs construction, modal scaling factor identification and flexibility identification, which are good candidates for structural damage detection and structural bearing capacity evaluation.
- Laboratory and numerical examples are conducted to verify the correctness of the proposed method, the predicted value from the proposed method agrees well with the reference value, which has successfully validated the proposed method.
- The effect of critical parameters on the identified results has also been conducted. Results indicates that road roughness, vehicle speed, vehicle weight, vehicle's stiffness and damping have little influence on flexibility identification, and although the relative error increases with the increase of measurement noise, the proposed method is still robust.

Acknowledgment

The authors are grateful for the financial support of the National Key R&D Program of China (No.: 2018YFC0705601), Jiangsu Distinguished Young Scholars Fund (No.: BK20160002) and National Science Foundation of China (Grant No. :51578139, 51778134). The first author appreciates the financial support from the Priority Academic Program Development of Jiangsu Higher Education Institutions (No.: 1105007002), and the Fundamental Research Funds for the Central Universities (Postgraduate Research＆Practice Innovation Program of Jiangsu Province, fund No: KYLX16_0246).

References

Adewuyi, A.P. and Wu, Z. (2015), "Vibration-based damage localization in flexural structures using normalized modal macrostrain techniques from limited measurements", *Comput. Aid Civil Infrastruct. Eng.*, **26**(3), 154-172. https://doi.org/10.1111/j.1467-8667.2010.00682.x.

Bayraktar, A., Altunışık, A.C., Sevim, B., Türker, T., Domaniç, A. and Taş, Y. (2009), "Vibration characteristics of Kömürhan highway bridge constructed with balanced cantilever method", *J. Perform. Construct. Faicilities ASCE*, **23**(2), 90-99. https://doi.org/10.1061/(ASCE)0887-3828(2009)23:2(90).

Brownjohn, J. M. W., Magalhaes, F., Caetano, E. and Cunha, A. (2010), "Ambient vibration re-testing and operational modal analysis of the humber bridge", *Eng. Struct.*, **32**(8), 2003-2018. https://doi.org/10.1016/j.engstruct.2010.02.034.

Brownjohn, J. M. W. (2007), "Structural health monitoring of civil infrastructure", *Philosophic. Transac. Math. Phys.Eng. Sci.*, **365**(1851), 589-622. https://doi.org/10.1098/rsta.2006.1925.

Brown, D.L. and Witter, M.C. (2011), "Review of recent developments in multiple reference impact testing (MRIT)", *Sound Vib.*, **45**(1), 97-114. https://doi.org/10.1007/978-1-4419-9834-7_10.

Catbas, F.N., Brown, D.L. and Aktan, A.E. (2004), "Parameter estimation for multiple-input multiple-output modal analysis of large structures", *J. Eng. Mech.*, **130**(8), 921-930. https://doi.org/10.1061/(ASCE)0733-9399(2004)130:8(921).

Catbas, F.N., Kijewski-Correa, T. and Aktan, E. (2013). *Structural Identification of Constructed Systems: Approaches, Methods, and Technologies for Effective Practice of St-Id*, *American Society of Civil Engineers*, ASCE, Reston, Virginia, USA.

De, Vitis J., Masceri, D., Aktan, A.E. and Moon F.L. (2013), "Rapid structural identification methods for highway bridges: Towards a greater understanding of large populations", *11th International Conference on Structural Safety & Reliability*, New York, United States, June.

Deng, L. and Cai, C.S. (2007), "Applications of fiber optic sensors in civil engineering", *Struct. Eng. Mech.*, **25**(5), 577-596. https://doi.org/10.12989/sem.2007.25.5.577.

Deng, L., Cai. C.S. (2009), "Identification of parameters of vehicles moving on bridges", *Eng. Struct.*, **31**(10), 2474-2485. https://doi.org/10.1016/j.engstruct.2009.06.005.

Dodds, C.J. and Robson, J.D. (1973), "The description of road surface roughness", *Sound Vib.*, **31**(2), 175-183.

https://doi.org/10.1016/S0022-460X(73)80373-6.

Fujino, Y., Siringoringo, D.M. and Abe, M. (2016), "Japan's experience on long-span bridges monitoring", *Struct. Monitor. Maintenance*, **3**(3), 233-257. http://dx.doi.org/10.12989/smm.2016.3.3.233.

Guo, W., Soibelman, L. and Garrett, J.H. (2009), "Visual pattern recognition supporting defect reporting and condition assessment of wastewater collection systems", *J. Comput. Civil Eng.*, **23**(3), 160-169. https://doi.org/10.1061/(ASCE)0887-3801(2009)23:3(160).

Guo, S., Zhang, X., Zhang, J., Zhou, Y., Moon, F. and Aktan, A.E. (2018), "Mobile impact testing of a simply-supported steel stringer bridge with reference-free measurement", *Eng. Struct.*, **159**, 66-74. https://doi.org/10.1016/j.engstruct.2017.12.020.

ISO 8608, (2016), "Mechanical vibration-road surface profiles-reporting of measured data", ISO, Geneva, Switzerland.

Kim, S., Pakzad, S., Culler, D., Demmel, J., Fenves, G., Glaser, S. and Turon, M. (2007), "Health monitoring of civil infrastructures using wireless sensor networks", *Proceedings of the 6th International Conference on Information Processing in Sensor Networks*, New York, April.

Liu, H. B., Zhang, Q. and Zhang, B.H. (2017), "Structural health monitoring of a newly built high-piled wharf in a harbor with fiber bragg grating sensor technology: Design and deployment", *Smart Struct. Syst.*, **20**(2), 163-173.

Lynch, J.P., Law, K.H., Kiremidjian, A.S., Carryer, E., Farrar, C.R., Sohn, H., Allen, D.W., Nadler, B. and Wait, J.R. (2004), "Design and performance validation of a wireless sensing unit for structural monitoring applications", *Struct. Eng. Mech.*, **17**(3), 3-4. https://doi.org/10.12989/sem.2004.17.3_4.393

Lynch, J.P. (2007), "An overview of wireless structural health monitoring for civil structures", *Philosophic. Transac. Math. Phys.Eng. Sci.,* **365**(1851), 345-372. https://doi.org/10.1098/rsta.2006.1932.

Mirzaee, A., Abbasnia, R., Shayanfar, M. (2018), "Simultaneous identification of damage in bridge under moving mass by Adjoint variable method", *Smart Struct. Syst.*, **21**(4), 449-467. https://doi.org/10.12989/sss.2018.21.4.449.

Nobahari, M. and Seyedpoor, S.M. (2013), "An efficient method for structural damage localization based on the concepts of flexibility matrix and strain energy of a structure", *Struct. Eng. Mech.*, **46**, 231-244. https://doi.org/10.12989/sem.2013.46.2.231.

Rahbari, R., Niu, J., Brownjohn, J.M.W. and Koo, K.Y. (2015), "Structural identification of humber bridge for performance prognosis", *Smart Struct. Syst.*, **15**(3), 665-682. https://doi.org/10.12989/sss.2015.15.3.665.

Sevim B., Atamturktur, S., Altunişik A.C., Bayraktar A. (2016), "Ambient vibration testing and seismic behavior of historical arch bridges under near and far fault ground motions", *Bullet. Earthq. Eng.*, **14**(1), 241-259. https://doi.org/10.1007/s10518-015-9810-6.

Soyoz, S. and Feng, M.Q. (2010), "Long-term monitoring and identification of bridge structural parameters", *Comput. Aid Civil Infrastruct. Eng.*, **24**(2), 82-92. https://doi.org/10.1111/j.1467-8667.2008.00572.x.

Sabato, A., Niezrecki, C. and Fortino, G. (2017), "Wireless mems-based accelerometer sensor boards for structural vibration monitoring: A review", *IEEE Sensors J.*, **PP**(99), 1. https://doi.org/10.1109/JSEN.2016.2630008.

Tian, Y., Zhang, J., Xia, Q. and Li, P. (2017), "Flexibility identification and deflection prediction of a three-span concrete box girder bridge using impacting test data", *Eng. Struct.*, **146**, 158-169. https://doi.org/10.1016/j.engstruct.2017.05.039.

Tian, Y., Zhang, J. and Yu, S. (2019), "Vision-based structural scaling factor and flexibility identification through mobile impact testing", *Mech. Syst. Signal Process.*, **122**, 387-402. https://doi.org/10.1016/j.ymssp.2018.12.029.

Toydemir B., Koçak A., Sevim B. and Zengin B. (2017), "Ambient vibration testing and seismic performance of precast I beam bridges on a high-speed railway line", *Steel Compos. Struct.*, 2**3**(5), 557-570. https://doi.org/10.12989/scs.2017.23.5.557.

Yang, Y.B. and Lin, C.W. (2005), "Vehicle-bridge interaction dynamics and potential applications", *Sound Vib.*, **284**(1), 205-226. https://doi.org/10.1016/j.jsv.2004.06.032.

Xiang, Z., Dai, X., Zhang, Y. and Lu, Q. (2010), "The tap-scan method for damage detection of bridge structures", *Interaction Multiscale Mech.*, **3**(2), 173-191. https://doi.org/10.12989/imm.2010.3.2.173.

Zhang, J., Guo, S. and Chen, X. (2014), "Mobile impact test data integrating for flexibility identification with only a single reference", *Comput. Aid Civil Infrastruct. Eng.*, **12**(3), 1-12. https://doi.org/10.1111/mice.12112.

Zhang, J., Guo, S.L. and Zhang, Q.Q. (2015), "Mobile impact testing for structural flexibility identification with only a single reference", *Comput. Aid Civil Infrastruct. Eng.*, **30**(9), 703-714. https://doi.org/10.1111/mice.12112.

Zhang, J. and Moon, F.L. (2012), "A new impact testing method for efficient structural flexibility identification", *Smart Mater. Struct.*, **21**(5), 1014-1022. https://doi.org/10.1088/0964-1726/21/5/055016.

Zhang, J. and Moon, F.L. (2012), "Novel structural flexibility identification in narrow frequency bands", *Smart Mater. Struct.*, **21**(12), 1-10. https://doi.org/10.1088/0964-1726/21/12/125020.

Zhang, J., Prader, J., Grimmelsman, K.A., Moon, F., Aktan, A.E. and Shama, A. (2013), "Experimental vibration analysis for structural identification of a long-span suspension bridge", *J. Eng. Mech.*, **139**(6), 748-759. https://doi.org/10.1061/(ASCE)EM.1943-7889.0000416.

PL